



**HAL**  
open science

## **Fretting fatigue crack initiation and propagation in Ti6Al4V sheets under tribocorrosive conditions of artificial seawater and physiological solutions**

Zeeshan Anjum, Masood Shah, Hassan Elahi, Mushtaq Khan, Mohammad Mujahid, Shahab Khushnood, Faisal Qayyum

### ► To cite this version:

Zeeshan Anjum, Masood Shah, Hassan Elahi, Mushtaq Khan, Mohammad Mujahid, et al.. Fretting fatigue crack initiation and propagation in Ti6Al4V sheets under tribocorrosive conditions of artificial seawater and physiological solutions. Proceedings of the Institution of Mechanical Engineers, Part L: Journal of Materials: Design and Applications, 2020, 234 (12), pp.1526-1534. 10.1177/1464420720946431 . hal-02919891

**HAL Id: hal-02919891**

**<https://imt-mines-albi.hal.science/hal-02919891>**

Submitted on 22 Oct 2020

**HAL** is a multi-disciplinary open access archive for the deposit and dissemination of scientific research documents, whether they are published or not. The documents may come from teaching and research institutions in France or abroad, or from public or private research centers.

L'archive ouverte pluridisciplinaire **HAL**, est destinée au dépôt et à la diffusion de documents scientifiques de niveau recherche, publiés ou non, émanant des établissements d'enseignement et de recherche français ou étrangers, des laboratoires publics ou privés.

# Fretting fatigue crack initiation and propagation in Ti6Al4V sheets under tribocorrosive conditions of artificial seawater and physiological solutions

Zeeshan Anjum<sup>1,2</sup>, Masood Shah<sup>1,3</sup>, Hassan Elahi<sup>4</sup> ,  
Mushtaq Khan<sup>5</sup>, Mohammad Mujahid<sup>6</sup>, Shahab Khushnood<sup>1</sup> and  
Faisal Qayyum<sup>7</sup>

## Abstract

The interaction of mechanical components experiencing relative movements and cyclic loads in a corrosive environment is known as fretting corrosion or tribocorrosion. In the current work, the mechanism of crack initiation and propagation in dovetail slots of Ti6Al4V samples (in contact with carbide rods) under fretting corrosion conditions was investigated. A newly developed test rig installed on a universal testing machine was used to conduct tests at 20 Hz frequency under 5 and 7.5 kN fretting loads. Tests were conducted at room temperature in 3.5% NaCl and phosphate-buffered saline solutions. Crack propagation in all samples was examined by a metallurgical microscope, and the detailed analysis of fractured samples was carried out by a scanning electron microscope. In comparison to dry conditions, early crack initiation and faster crack propagation were observed in salt and physiological solution environments. Colored spots and large amounts of chlorine, sodium, and oxygen were found around cracks, and plastically deformed regions in the 3.5% NaCl environment provided the evidence of a corrosive attack. Large amounts of oxygen, phosphorous, chlorine, potassium, and sodium were detected in the phosphate-buffered saline environment.

## Keywords

Fretting fatigue, titanium, novel testing method, microscopic analysis, crack propagation rate

## Introduction

Tribocorrosion or fretting corrosion occurs when mechanical components undergo relative slips in a corrosive environment. This phenomenon is observed in different applications, such as engine components in contact with lubricants, eyeglass frames, artificial implants (hip and knee joints), and pump components.<sup>1</sup> Fretting corrosion results in metal degradation due to the combined effect of mechanical wear and chemical oxidation.<sup>2</sup> Corrosion and wear mechanisms are dependent on each other in a complicated way.<sup>3</sup> It is generally observed that under fretting tribological conditions, the metal degradation rate gets enhanced due to the combined effect of chemical reactions and wear, resulting in an early fracture of components.<sup>4,5</sup> Therefore, a correct prediction of the initiation and growth of fretting-initiated cracks is the key to improved fretting designs. Theoretically, the Smith–Watson–Topper method can be used to

---

<sup>1</sup>Department of Mechanical Engineering, University of Engineering and Technology Taxila, Pakistan

<sup>2</sup>Department of Mechanical Engineering, Mirpur University of Science and Technology, Mirpur, Pakistan

<sup>3</sup>INSA, UPS, Mines Albi, ISAE, Institut Clément Ader (ICA), Université de Toulouse, France

<sup>4</sup>Department of Mechanical and Aerospace Engineering, Sapienza University of Rome, Italy

<sup>5</sup>School of Mechanical and Manufacturing Engineering, National University of Sciences and Technology, Islamabad, Pakistan

<sup>6</sup>School of Chemical and Materials Engineering, National University of Sciences and Technology, Islamabad, Pakistan

<sup>7</sup>Institute of Metal Forming, Technische Universität Bergakademie Freiberg, Germany

### Corresponding author:

Hassan Elahi, Department of Mechanical and Aerospace Engineering, Sapienza University of Rome, Italy.  
Email: hassan.elahi@uniroma1.it

predict crack initiation, and fracture mechanics<sup>6–9</sup> and finite element approaches<sup>10–15</sup> are applied to predict crack propagation in a component.

Titanium and its alloys exhibit excellent corrosion resistance by forming 2–5 nm thick uniform oxide layers on component surfaces.<sup>16</sup> However, these thin oxide layers are highly susceptible to cracking under fretting fatigue and harsh tribological conditions.<sup>17</sup> Mechanical parameters and electrochemical conditions greatly affect the fretting corrosion behavior of Ti6Al4V.<sup>18</sup>

In previous studies, the fracture and wear in Ti6Al4V samples under fretting fatigue loads have been investigated using sophisticated fixtures consisting of fretting pads and flat or dog-bone-shaped samples.<sup>19–21</sup> Different contact configurations, such as balls on flat samples,<sup>22</sup> flat pads on flat samples,<sup>7</sup> and spherical pads on flat samples<sup>23</sup> have been applied. The fretting wear mechanism of Ti6Al4V samples in a corrosive environment is mainly investigated by conventional electrochemical setups.<sup>24–26</sup>

The fracture mechanism and corrosion behavior of Ti6Al4V under fretting fatigue have been explored separately; hence, not much literature can be found on the combined effect of fracture and corrosion in Ti6Al4V samples under fretting loads. In the present work, fracture and corrosion phenomena in Ti6Al4V samples under fretting corrosion conditions were investigated.

In this research work, a new test setup was developed to investigate crack initiation, propagation, and arrest under fretting fatigue loads in corrosive environments. This test setup is much simpler in construction and operation as compared to previous setups used in fretting wear and corrosion experiments. This setup also offers the ease of observation of micro-cracks during experiments. Tests were carried out using a pin-in-dovetail contact configuration of Ti6Al4V specimens and carbide rods at room temperature and 20 Hz frequency in 3.5% NaCl and phosphate-buffered saline (PBS) solutions<sup>27</sup> under 5 and 7.5 kN loads. Crack propagation in the samples was measured by a metallurgical microscope. The detailed fractographic and tribocorrosion analysis was performed by a scanning electron microscope (SEM), and the obtained results were compared with the findings (tests were carried out under dry ambient conditions) of Anjum et al.<sup>28</sup>

## Experimentation

### Sample preparation

Ti6Al4V sheets (American Standard for Testing of Materials Grade 5 titanium alloy) with a thickness of 2 mm were used for sample preparation. Rectangular samples having one dovetail and one circular hole were machined by a CNC milling machine.<sup>28</sup> After machining, all samples were cleaned

by abrasive papers to remove scratches, especially around dovetail slots.

The samples had a width of 45 mm and a height of 74 mm (Figure 1(a)). Carbide rods had a diameter of 12 mm and a length of 87.5 mm, and a 3 mm slot was present on either end of these rods to insert clamping pins (Figure 1(b)). A clearance of 1 mm existed between circular holes and dovetail slots to cause relative slips during loading cycles.

The cylinder on flat surface contact configuration (line contact) was used for carbide rods and dovetail slots, and the rolling of carbide rods was avoided with the help of the frictional effect (pure Hertzian contact). The Hertzian pressure ( $P_h$ ) and the contact width ( $b$ ) were calculated by equations (1) and (2), respectively<sup>29</sup>

$$P_h = 0.591 \sqrt{\frac{F_N}{L \Delta} \left( \frac{1}{R_1} + \frac{1}{R_2} \right)} \quad (1)$$

$$b = 1.076 \sqrt{\frac{F_N \Delta}{L \left( \frac{1}{R_1} + \frac{1}{R_2} \right)}} \quad (2)$$

where

$$\Delta = \frac{1}{E_1} (1 - \nu_1^2) + \frac{1}{E_2} (1 - \nu_2^2) \quad (3)$$

The maximum shear stress ( $\tau_{\max}$ ) was calculated by equation (4), and it occurred beneath the surface at a depth of 0.786 of the contact width ( $b$ ) and on planes inclining at 45° to the load axis.<sup>29</sup> Hertzian contact parameters calculated for the current loading

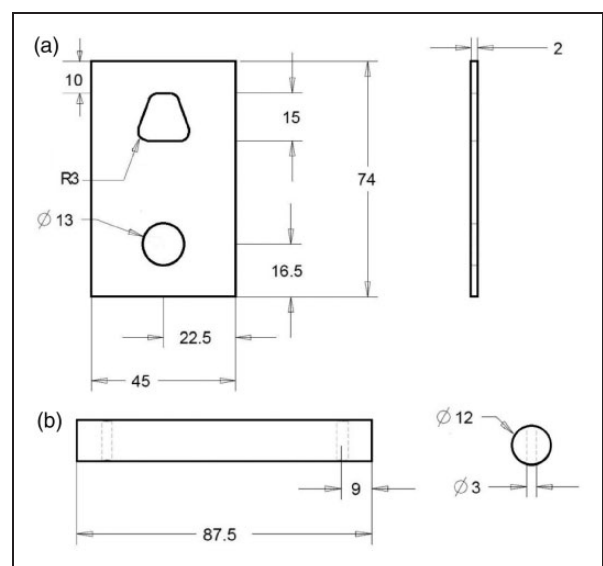


**Figure 1.** Schematic diagrams of (a) a Ti6Al4V sample having a dovetail slot and a circular hole and (b) a carbide rod having two holes to insert clamping pins. (All dimensions are in mm.)

conditions are presented in Table 1

$$\tau_{\max} = 0.295 P_h \quad (4)$$

The location of the maximum shear stress beneath the surface was calculated by equation (5)

$$x = 0.786 b \quad (5)$$

### Experimental setup

A previously developed fretting fatigue test rig<sup>28</sup> was modified for the current tribocorrosion experiment. The test setup consisted of two H13 clevis grips, washers, and two rods with external threads. In order to carry out experiments under different environmental conditions, the test setup was modified by tungsten inert gas welding a container made from stainless steel (SS304) sheets having 3 mm wall thickness and 6 mm base thickness with a clevis grip. It had a height, length, and width of 80, 156, and 86 mm, respectively. A discharge pipe of 12 mm diameter was welded at one side of the container to remove the fluid after tests. The container was designed with a volumetric capacity of 1 L.

Tests were carried out at room temperature by attaching the constructed rig to a universal testing machine (Material Testing System (MTS) 810) having

a maximum load capacity of 100 kN (Figure 2). Samples were mounted and loaded with the help of carbide rods passing through dovetail slots and circular holes. Dovetail slots were mounted with the lower clevis grip through carbide rods and remained immersed in the corrosive solution during experiments, whereas circular holes were mounted with the upper clevis grip through carbide rods (Figure 3). Constant

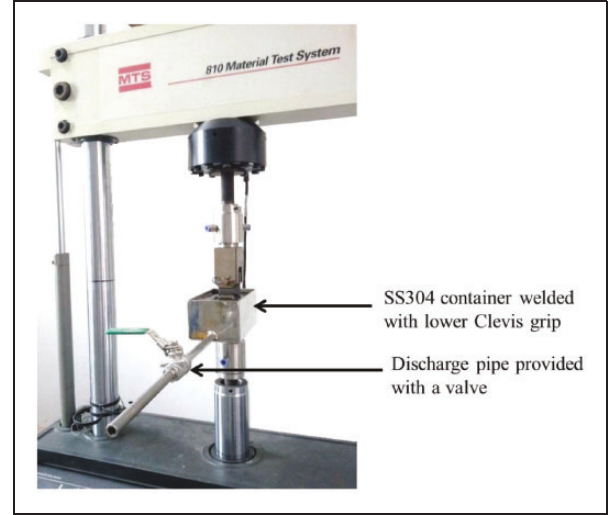


**Figure 2.** Arrangement of newly developed test rig on universal testing machine, MTS 810.

**Table 1.** Summary of Hertzian contact parameters.

Load	Normal component	Hertzian pressure	Contact width	Maximum shear stress	Location of maximum shear below the surface
$P$	$F_N = P \cos 70^\circ$	$P_h$	$b$	$\tau_{\max}$	$x$
kN	kN	GPa	mm	MPa	mm
5	1.71	2.34	0.231	690	0.18
7.5	2.565	2.86	0.283	843	0.22

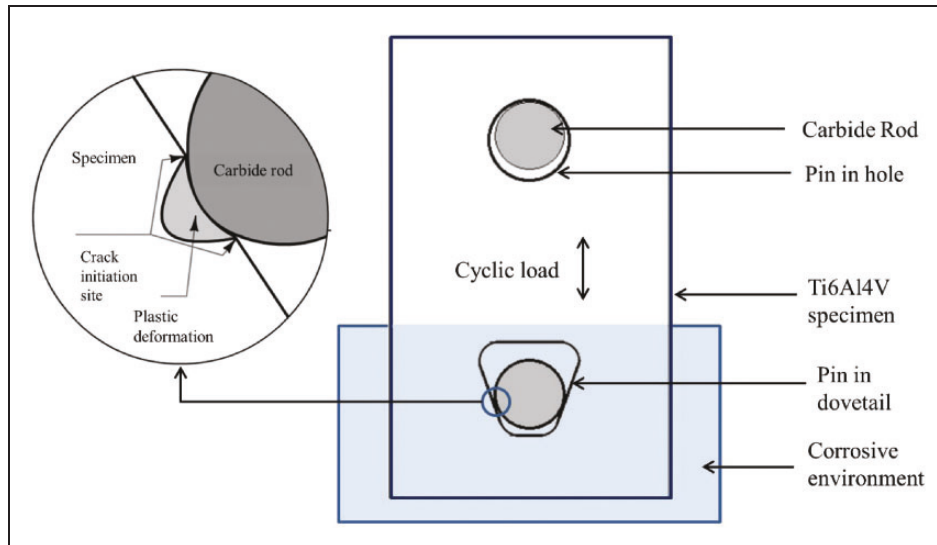


**Figure 3.** Schematic diagram showing immersion of specimen during experimentation while inset diagram shows plastic deformation and crack initiation sites at the edges of the contact.

amplitude tension–tension axial fatigue loads of 5 and 7.5 kN with a load ratio of  $R=0.1$  were applied with the help of the lower clevis grip and carbide rods, and the frequency was kept constant at 20 Hz.

Tests were carried out in both 3.5% NaCl and PBS solutions.<sup>27</sup> The contact under investigation (Ti6Al4V internal dovetail slot and carbide rod) remained completely immersed in corrosive solutions during experiments (Figure 3).

Crack propagation in the samples was measured after regular intervals by a metallurgical microscope (Olympus DP-20). The microscopic analysis of fractured samples was carried out by a SEM (TESCAN VEGA3) after cleaning the samples in an ultrasonic bath.

## Results

Plastic deformation was observed in all samples at the contact region. It was observed that cracks initiated at the edges and on both sides of the contact (Figure 3).

### Crack initiation and propagation

Four major cracks initiated in all samples—two at either side of the contact: right top (RT), right bottom (RB), left top (LT), left bottom (LB) (Figure 4(a)). Moreover, plastic deformation was observed in the tested samples (Figure 4(b)). A few minor cracks with much shorter lengths also appeared near the edges of the contact; however, they did not propagate. Among these four major cracks, Crack-LT and Crack-RT propagated longer into the samples. It happened because the cracks at the lower edge of the contact underwent compression, whereas the cracks at the top edge of the contact experienced tension.

These cracks initiated in mode II<sup>30,31</sup> at an angle of approximately 45° to the contact surface, and propagated perpendicularly to the surface in tensile mode

until the phenomenon of crack arrest occurred due to the reduction of the stress intensity factor.<sup>28</sup> The propagation of the cracks at the top edge (Crack-LT and Crack-RT) in salt and PBS environments and under dry conditions<sup>28</sup> at 5 and 7.5 kN loads are presented in Figures 5 and 6, respectively.

It is evident that the presence of the salt environment caused a decrease in fatigue strength.<sup>32</sup> Cracks were generated due to hydrogen embrittlement resulting from the formation of halogen acid under the pyro-hydrolysis of salts.<sup>25,33</sup> The continuous availability of the HCl environment further promoted the formation of monoatomic hydrogen, causing hydrogen embrittlement to help cracks propagate under stress.

The crack propagation rate in the salt environment was found to be higher (up to 14.5%) than that in the non-corrosive environment under both 5 and 7.5 kN loads. The crack propagation rate in the PBS environment was about 46.6% higher than that at ambient conditions under similar loading conditions. The maximum crack length of about 800  $\mu\text{m}$  was observed in the PBS environment at 7.5 kN load, and it is  $\sim 28\%$  greater than that observed in the 3.5% NaCl solution under similar loading conditions.

A comparison of average crack propagation and average crack propagation rate in 3.5% NaCl, PBS, and non-corrosive environments is presented in Figure 7. It is evident that the average crack length and crack propagation rate in corrosive environments were much higher and crack arrest occurred after  $\sim 160,000$  cycles.

### Scanning electron microscopy

In the NaCl environment, blue spots were observed around fractured surfaces due to the increased amount of chlorine, oxygen, and sodium.<sup>25,34,35</sup> The chemical mapping of fractured specimens around these blue spots by SEM revealed the presence of chlorine, oxygen, and sodium (Figure 8).

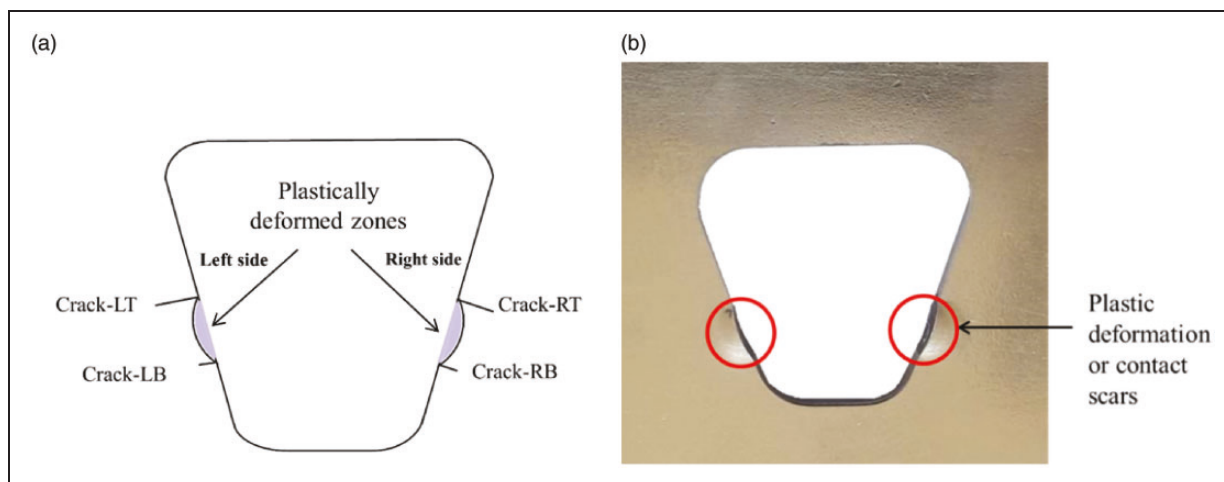


**Figure 4.** Plastic deformation and major cracks observed. (a) Schematic diagram; (b) tested sample.

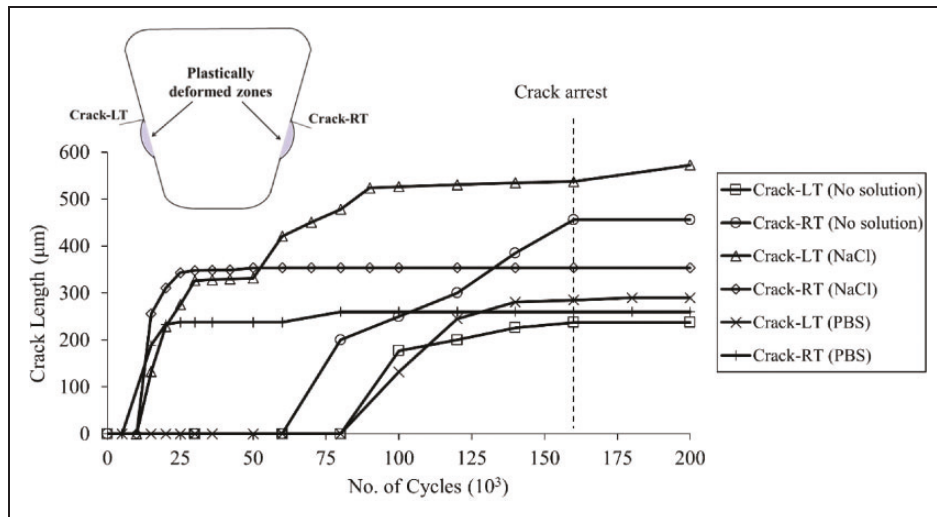


**Figure 5.** Comparison of the propagation of cracks at the top edge in NaCl and PBS solutions with non-corrosive environment observed earlier<sup>28</sup> at 5 kN fatigue load.

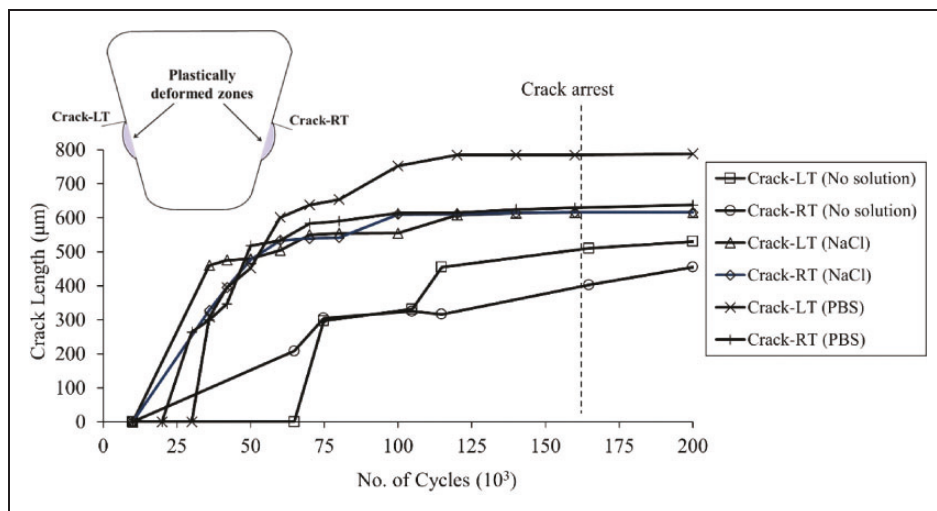


**Figure 6.** Comparison of the propagation of cracks at the top edge in NaCl and PBS solutions with non-corrosive environment observed earlier<sup>28</sup> at 7.5 kN fatigue load.

The concentrations of sodium and chlorine were lower than the oxygen concentration along the crack length. The line data obtained for the blue-colored region near the crack (Figure 9(a)) also revealed the presence of these elements while the amount of oxygen was higher than those of sodium and chlorine (Figure 9(b)).

Excessive oxidation was observed in the samples tested under the PBS environment. SEM images of these samples manifested a dark region near the contact zone adjacent to the machined surface and a less dark region away from the machined surface. The chemical mapping around the contact zone and the cracked path revealed the presence of oxygen, phosphorous, chlorine, potassium, and sodium (Figure 10). A similar pitting corrosion phenomenon was previously reported during the electrochemical study of titanium alloys in PBS solutions due to the presence of phosphate anions.<sup>27,36</sup>

## Discussion

The mechanism of crack initiation and propagation in Ti6Al4V pin-in-dovetail samples (in contact with carbide rods) under fretting corrosion conditions were investigated. A new testing setup was developed to perform fretting tests at 5 and 7.5 kN under both salt and physiological solution environments.

Four major cracks were formed at the edges of the contact region due to fretting.<sup>28,31</sup> Titanium formed a thin oxide layer on the component surface to prevent corrosion.<sup>37</sup> Plastic deformation in the NaCl solution broke this thin layer and exposed the bare metal to the corrosive environment, thus enhancing the crack propagation rate. Blue spots were observed around cracks and along the contact zone in the salt environment due to the excessive amount of oxygen, chlorine, and sodium which is also reported by previous researchers.<sup>25,34</sup> It is believed that hydrogen

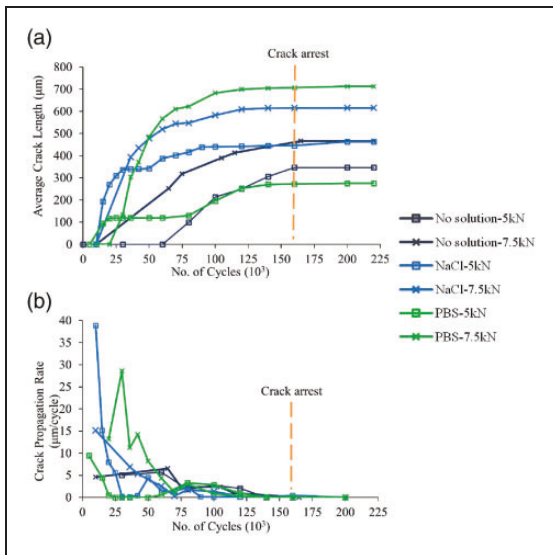


**Figure 7.** Comparison of (a) average crack propagation and (b) average crack propagation rate in non-corrosive, 3.5% NaCl and PBS environments.

embrittlement is responsible for the enhanced crack propagation in titanium alloys under salt environments.<sup>38,39</sup>

Colored spots were also observed in the PBS environment; however, they were more intense in color than those observed in the NaCl environment. The protective oxide layer ruptured earlier in this environment, thus in comparison to NaCl or dry conditions, cracks propagated longer in the PBS environment. The energy dispersive X-ray spectroscopy (EDX) analysis revealed the presence of excess oxygen, chlorine, phosphorous, sodium, and potassium along the colored regions. The presence of these elements caused cracks to propagate farther and also resulted in the initiation of minor cracks at contact edges near major cracks.

In both these environments, crack initiation occurred in the shear mode at 45° to the contact surface, and crack propagation occurred in the tensile mode. In comparison to dry conditions, both NaCl

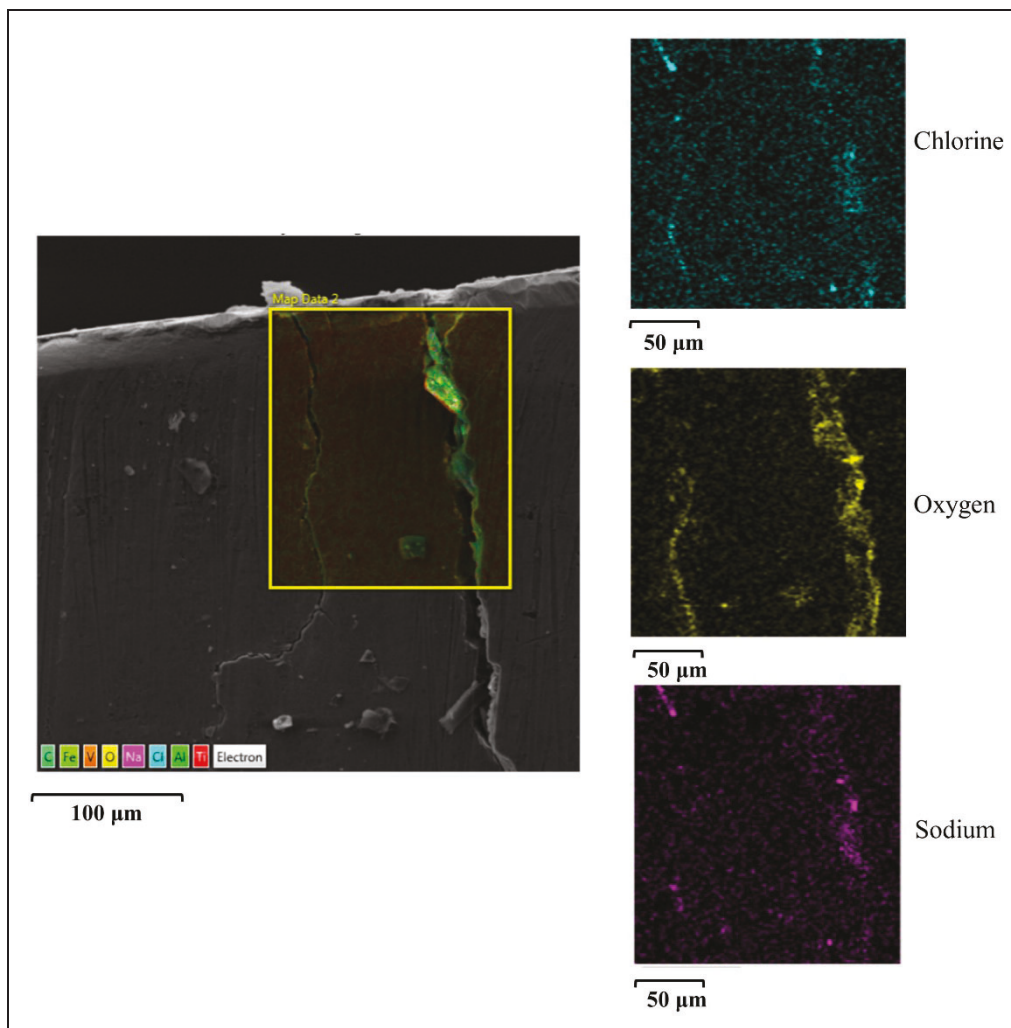


**Figure 8.** SEM-EDX chemical mapping near crack initiation zone in 3.5% NaCl solution.

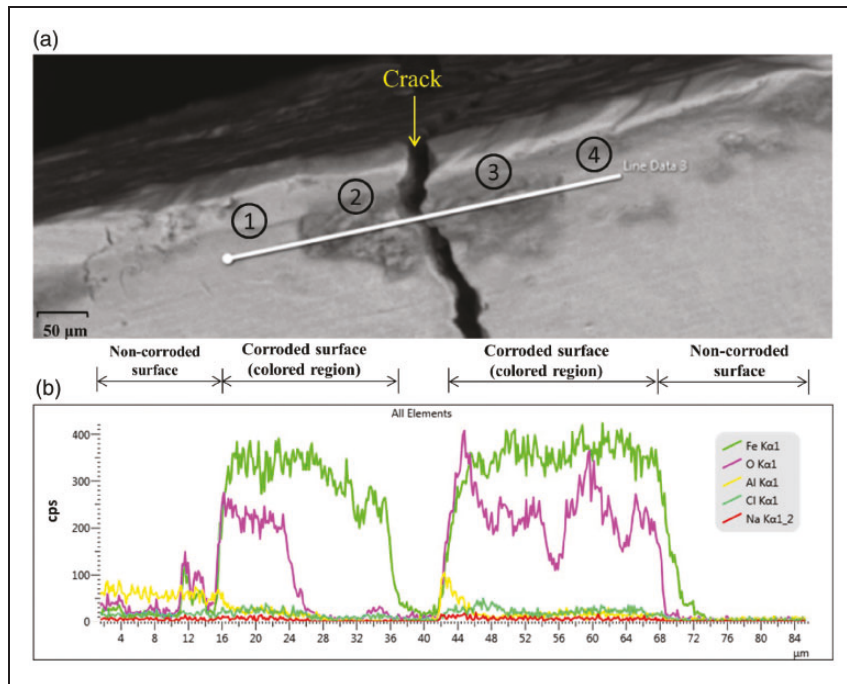


**Figure 9.** (a) Line data obtained for the blue colored region near crack and (b) graph exhibiting element concentrations in the respective regions.

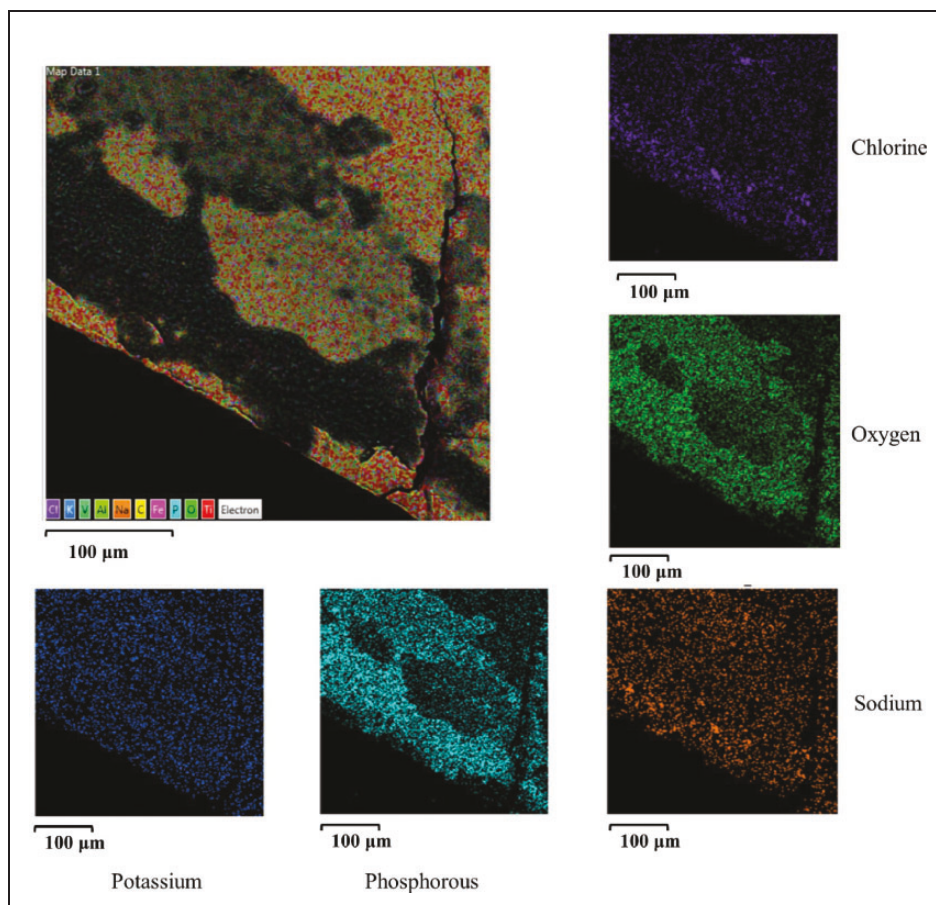


**Figure 10.** SEM-EDX chemical mapping of the fractured sample in the PBS environment.

and PBS corrosive environments caused earlier crack initiation and shorter sample life.<sup>4,40–43</sup> It happened because chemical reactions ruptured the protective oxide layer much earlier and exposed the bare metal.

## Conclusions

The main inferences of the present experiment are presented below.

1. Four major cracks at the edges of the contact region were observed in all samples under both salt and physiological environments.
2. The crack propagation rate in the salt environment was higher (up to 14.5%) than that in dry conditions at both 5 and 7.5 kN fatigue loads.
3. Crack propagation is 28% and 46.6% greater in the PBS environment as compared with 3.5% NaCl and in dry test conditions, respectively, at 7.5 kN fatigue load.
4. Intense dark spots (pits) were observed around fractured surfaces due to excessive corrosion, causing earlier crack initiation and prolonged crack propagation.
5. Colored spots around cracks were found due to the increased amounts of oxygen, chlorine, and sodium in the NaCl environment. In contrast, the presence of oxygen, phosphorous, chlorine, potassium, and sodium was detected around fractured surfaces in the PBS environment.

## Acknowledgments

The authors acknowledge the research facility provided by Fracture Mechanics and Fatigue Laboratory, Department of Mechanical Engineering, University of Engineering and Technology Taxila, Punjab, Pakistan. Authors also acknowledge the technical support provided by Mr Qaiser, Mr Asad Maqsood, and Mr Aman Ullah during the test rig fabrication and conduction of experiments.

## Declaration of conflicting interests

The author(s) declared no potential conflicts of interest with respect to the research, authorship, and/or publication of this article.

## Funding

The author(s) received no financial support for the research, authorship, and/or publication of this article.

## ORCID iD

Hassan Elahi  <https://orcid.org/0000-0001-6836-604X>

## References

1. Takadom J. *Materials and surface engineering in tribology*. New York, NY: John Wiley & Sons, 2013.
2. Committee AIH. *Friction, lubrication, and wear technology*. Materials Park, OH: ASM International, 1992.
3. Barril S, Mischler S and Landolt D. Electrochemical effects on the fretting corrosion behaviour of Ti6Al4V in 0.9% sodium chloride solution. *Wear* 2005; 259: 282–291.
4. Manhabosco TM, Tamborim SM, dos Santos CB, et al. Tribological, electrochemical and tribo-electrochemical characterization of bare and nitrided Ti6Al4V in simulated body fluid solution. *Corros Sci* 2011; 53: 1786–1793.
5. Diomidis N, Mischler S, More N, et al. Tribo-electrochemical characterization of metallic biomaterials for total joint replacement. *Acta Biomater* 2012; 8: 852–859.
6. Ding J, Sum WS, Sabesan R, et al. Fretting fatigue predictions in a complex coupling. *Int J Fatigue* 2007; 29: 1229–1244.
7. Wei D-S, Yuan S-H and Wang Y-R. Failure analysis of dovetail assemblies under fretting load. *Eng Fail Anal* 2012; 26: 381–396.
8. Golden PJ and Grandt AF Jr. Fracture mechanics based fretting fatigue life predictions in Ti-6Al-4V. *Eng Fract Mech* 2004; 71: 2229–2243.
9. Ullah M, Wu CS and Qayyum F. Prediction of crack tip plasticity induced due to variation in solidification rate of weld pool and its effect on fatigue crack propagation rate (FCPR). *J Mech Sci Technol* 2018; 32: 3625–3635.
10. Wei D-S, Wang Y-R and Yang X-G. Analysis of failure behaviors of dovetail assemblies due to high gradient stress under contact loading. *Eng Fail Anal* 2011; 18: 314–324.
11. Barsoum I, Khan F and Barsoum Z. Analysis of the torsional strength of hardened splined shafts. *Mater Des* 2014; 54: 130–136.
12. Swati R, Wen L, Elahi H, et al. Extended finite element method (XFEM) analysis of fiber reinforced composites for prediction of micro-crack propagation and delaminations in progressive damage: a review. *Microsyst Technol* 2019; 25: 747–763.
13. Memmolo V, Elahi H, Eugeni M, et al. Experimental and numerical investigation of PZT response in composite structures with variable degradation levels. *J Mater Eng Perform* 2019; 28: 3239–3246.
14. Qayyum F, Guk S, Prüger S, et al. Investigating the local deformation and transformation behavior of sintered X3CrMnNi16-7-6 TRIP steel using a calibrated crystal plasticity-based numerical simulation model. *Int J Mater Res*. 2020; 111: 392–404.
15. Mukhtar F, Qayyum F, Elahi H, et al. Studying the effect of thermal fatigue on multiple cracks propagating in an SS316L thin flange on a shaft specimen using a multi-physics numerical simulation model. *Strojnikski Vestnik J Mech Eng* 2019; 65: 565–573.
16. Marino CE, de Oliveira EM, Rocha-Filho RC, et al. On the stability of thin-anodic-oxide films of titanium in acid phosphoric media. *Corros Sci* 2001; 43: 1465–1476.
17. Totolin V, Pejaković V, Csanyi T, et al. Surface engineering of Ti6Al4V surfaces for enhanced tribocorrosion performance in artificial seawater. *Mater Des* 2016; 104: 10–18.
18. Barril S, Debaud N, Mischler S, et al. A tribo-electrochemical apparatus for in vitro investigation of fretting-corrosion of metallic implant materials. *Wear* 2002; 252: 744–754.

19. Lykins CD, Mall S and Jain VK. Combined experimental–numerical investigation of fretting fatigue crack initiation. *Int J Fatigue* 2001; 23: 703–711.
20. Teng J and Sato K. In situ observations of fretting wear behavior in PMMA/steel model. *Mater Des* 2004; 25: 471–478.
21. Golden PJ. Development of a dovetail fretting fatigue fixture for turbine engine materials. *Int J Fatigue* 2009; 31: 620–628.
22. Anand Kumar S, Ganesh Sundara Raman S, Sankara Narayanan TSN, et al. prediction of fretting wear behavior of surface mechanical attrition treated Ti–6Al–4V using artificial neural network. *Mater Des* 2013; 49: 992–999.
23. Venkatesh T, Conner B, Suresh S, et al. An experimental investigation of fretting fatigue in Ti-6Al-4V: the role of contact conditions and microstructure. *Metall Mater Trans A* 2001; 32: 1131–1146.
24. Benea L, Danaila E and Ponthiaux P. Effect of titania anodic formation and hydroxyapatite electrodeposition on electrochemical behaviour of Ti–6Al–4V alloy under fretting conditions for biomedical applications. *Corros Sci* 2015; 91: 262–271.
25. Chapman T, Chater R, Saunders E, et al. Environmentally assisted fatigue crack nucleation in Ti–6Al–2Sn–4Zr–6Mo. *Corros Sci* 2015; 96: 87–101.
26. Chen J, Zhang Q, Li Q-A, et al. Corrosion and tribocorrosion behaviors of AISI 316 stainless steel and Ti6Al4V alloys in artificial seawater. *Trans Nonferrous Met Soc China* 2014; 24: 1022–1031.
27. Aziz-Kerrzo M, Conroy KG, Fenelon AM, et al. Electrochemical studies on the stability and corrosion resistance of titanium-based implant materials. *Biomaterials* 2001; 22: 1531–1539.
28. Anjum Z, Qayyum F, Khushnood S, et al. prediction of non-propagating fretting fatigue cracks in Ti6Al4V sheet tested under pin-in-dovetail configuration: experimentation and numerical simulation. *Mater Des* 2015; 87: 750–758.
29. Hearn EJ. *Mechanics of materials 2: The mechanics of elastic and plastic deformation of solids and structural materials*. Amsterdam: Elsevier, 1997.
30. Mutoh Y and Xu J-Q. Fracture mechanics approach to fretting fatigue and problems to be solved. *Tribol Int* 2003; 36: 99–107.
31. Mukhtar F, Qayyum F, Anjum Z, et al. effect of chrome plating and varying hardness on the fretting fatigue life of AISI D2 components. *Wear* 2019; 418: 215–225.
32. Jiang H, Cong Y, Zhang X, et al. Fatigue degradation after salt spray ageing of electromagnetically riveted joints for CFRP/Al hybrid structure. *Mater Des* 2018; 142: 297–307.
33. Araújo J, Susmel L, Pires M, et al. A multiaxial stress-based critical distance methodology to estimate fretting fatigue life. *Tribol Int* 2017; 108: 2–6.
34. Donachie M, Danesi W and Pinkowish A. Effects of salt atmosphere on crack sensitivity of commercial titanium alloys at 600 to 900 F. In: *Stress-corrosion cracking of titanium*. West Conshohocken, PA: ASTM International, 1966.
35. Saunders E, Chapman T, Walker A, et al. Understanding the “blue spot”: sodium chloride hot salt stress-corrosion cracking in titanium-6246 during fatigue testing at low pressure. *Eng Fail Anal* 2016; 61: 2–20.
36. Runa MJ, Mathew MT and Rocha LA. Tribocorrosion response of the Ti6Al4V alloys commonly used in femoral stems. *Tribol Int* 2013; 68: 85–93.
37. Pejaković V, Totolin V and Ripoll MR. Tribocorrosion behaviour of Ti6Al4V in artificial seawater at low contact pressures. *Tribol Int* 2018; 119: 55–65.
38. Zhao PC, Li SX, Jia YF, et al. Very high-cycle fatigue behaviour of Ti-6Al-4V alloy under corrosive environment. *Fatigue Fract Eng Mater Struct* 2018; 41: 881–893.
39. Tal-Gutelmacher E and Eliezer D. Hydrogen-assisted degradation of titanium based alloys. *Mater Trans* 2004; 45: 1594–1600.
40. Diomidis N, Celis J-P, Ponthiaux P, et al. Tribocorrosion of stainless steel in sulfuric acid: identification of corrosion–wear components and effect of contact area. *Wear* 2010; 269: 93–103.
41. Contu F, Elsener B and Böhni H. A study of the potentials achieved during mechanical abrasion and the repassivation rate of titanium and Ti6Al4V in inorganic buffer solutions and bovine serum. *Electrochim Acta* 2004; 50: 33–41.
42. Milošev I, Metikoš-Huković M and Strehblow H-H. Passive film on orthopaedic TiAlV alloy formed in physiological solution investigated by X-ray photoelectron spectroscopy. *Biomaterials* 2000; 21: 2103–2113.
43. Yu C, Zhu S, Wei D, et al. Oxidation and H<sub>2</sub>O/NaCl-induced corrosion behavior of sputtered Ni–Si coatings on Ti6Al4V at 600–650°C. *Surf Coat Technol* 2007; 201: 7530–7537.

## Appendix

### Notation

$b$	contact width
$E_1$ & $E_2$	= modulus of elasticity of carbide and titanium, respectively
$F_N$	normal component of applied load
$F_T$	tangential component of applied load
$L$	contact length
$P$	axial load
$P_h$	Hertzian pressure
$R$	stress ratio
$\vartheta_1$ & $\vartheta_2$	Poisson's ratio of carbide and titanium, respectively
$R_1$ & $R_2$	Radii of carbide rod and titanium flat plate sample respectively